Understanding Dense Active Nematics from Microscopic Models

Aurelio Patelli,[1] Ilyas Djafer-Cherif,[1,2] Igor S. Aranson,[3] Eric Bertin,[4] and Hugues Chaté[1,5,6]
[1]Service de Physique de l'Etat Condensé, CEA, CNRS, Université Paris-Saclay, CEA-Saclay, 91191 Gif-sur-Yvette, France
[2]School of Mathematics, University of Bristol, Bristol BS8 1TW, United Kingdom
[3]Department of Biomedical Engineering, Pennsylvania State University, University Park, Pennsylvania 16802, USA
[4]Univ. Grenoble Alpes, CNRS, LIPhy, 38000 Grenoble, France
[5]Computational Science Research Center, Beijing 100094, China
[6]LPTMC, Sorbonne Université, CNRS, 75005 Paris, France

(Received 20 May 2019; revised manuscript received 13 September 2019; published 18 December 2019)

We study dry, dense active nematics at both particle and continuous levels. Specifically, extending the Boltzmann-Ginzburg-Landau approach, we derive well-behaved hydrodynamic equations from a Vicsek-style model with nematic alignment and pairwise repulsion. An extensive study of the phase diagram shows qualitative agreement between the two levels of description. We find in particular that the dynamics of topological defects strongly depends on parameters and can lead to "arch" solutions forming a globally polar, smecticlike arrangement of Néel walls. We show how these configurations are at the origin of the defect ordered states reported previously. This work offers a detailed understanding of the theoretical description of dense active nematics directly rooted in their microscopic dynamics.

DOI: 10.1103/PhysRevLett.123.258001

Active nematics (collections of self-propelled elongated particles aligning by collisions) has been the subject of rather intense theoretical attention [1–21]. This flurry of papers was largely triggered by a few remarkable experiments [22–31]—see also [32,33] for recent reviews. In particular, Dogic *et al.* [22] studied a suspension of bundles of stabilized microtubules and clusters of kinesin motor proteins sandwiched at an oil-water interface. This revealed sustained regimes of "nematic turbulence" with prominent motion of $\pm\frac{1}{2}$ topological defects, including intriguing "defect ordered states" in which the intrinsic orientations of $+\frac{1}{2}$ defects seem to be globally aligned.

Most theoretical efforts towards accounting for these remarkable experiments fall into two categories: microscopic, active particle models [3,22,34] and continuum descriptions in terms of deterministic hydrodynamic equations [5,8,9,11]. The microscopic models are mostly "dry"; i.e., they neglect the fluid surrounding the active particles, while mostly "wet" continuous descriptions, i.e., including a Stokes equation describing this fluid, have been considered. Dry continuous descriptions have also been written by enslaving the fluid [10,12,13]. While all these works had some success in accounting for experimentally observed properties, they lack a direct connection between the microscopic and macroscopic levels: The proposed continuous descriptions have not been studied in parallel to particle-based models. It is thus impossible to relate clearly their many parameters to those of any underlying microscopic dynamics.

In this Letter, we bridge the gap between particle-based models and continuous theories for dense active-nematics systems, focusing on the dry case. Extending the Boltzmann-Ginzburg-Landau approach of [35–37], we derive well-behaved hydrodynamic equations from a Vicsek-style active-nematics model with alignment and repulsion interactions. An extensive study of the phase diagrams of both particle model and hydrodynamic equations (varying key parameters of the microscopic dynamics) shows qualitative agreement between the two description levels. Among our salient results, we find that the dynamics of topological defects strongly depends on specific parameters. We also uncover "arch" solutions forming a globally polar, smecticlike arrangement of Néel walls that coexist with the homogeneous nematic state in large regions of parameter space. We show them to be at the origin of "defect ordered states" reported previously in [13,22]. Our work offers an understanding of the theoretical description of dense active nematics directly rooted in their microscopic dynamics and a unified account of previous partial results.

The microscopic, dry models proposed so far for dense active nematics rely on volume exclusion effects between elongated particles [3,22]. Here, we use a Vicsek-style model instead, where pointwise particles interact with those within a fixed distance [38,39]. This makes both the derivation of hydrodynamic equations and an extensive numerical study easier. Specifically, we study a variant of the model introduced in [40] for the study of active smectics. We consider point particles moving at a constant speed v_0 along the unit vector $\mathbf{e}(\theta)$ defined by their heading θ in a rectangular domain of size $L_x \times L_y$ with periodic boundary conditions. At discrete unit time steps, position $\mathbf{r}_i$ and heading θ_i of particle i are updated according to

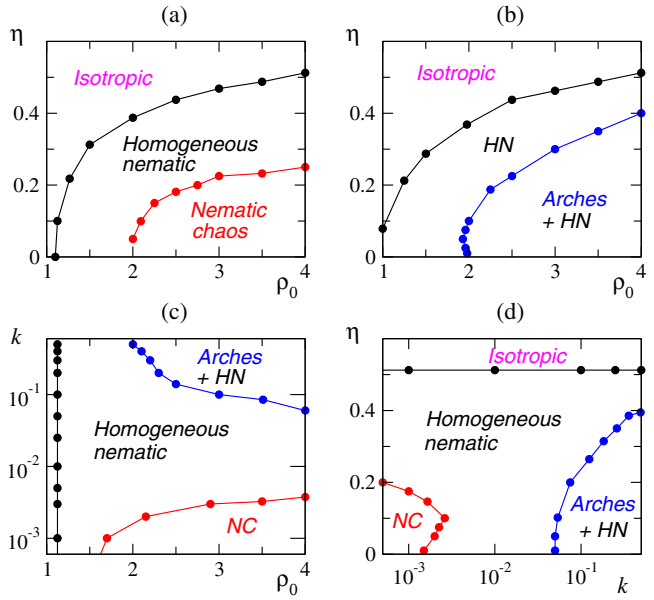

FIG. 1. Phase diagram of the particle model ($\beta = 0.5$, $v_0 = 0.3$, 256×256 periodic box). (a),(b) (ρ_0, η) plane for the rods ($k = 0$) and active-nematics ($k = 0.5$) cases. (c) (ρ_0, k) plane at $\eta = 0.1$. (d) (k, η) plane at $\rho_0 = 4$.

$$\mathbf{r}_i^{t+1} = \mathbf{r}_i^t + v_0 \mathbf{e}(\theta_i^{t+1}), \tag{1}$$

$$\theta_i^{t+1} = \arg[\epsilon_t \langle \mathrm{sgn}[\cos(\theta_i^t - \theta_j^t)] \mathbf{e}(\theta_j^t) \rangle_j + \beta \langle \hat{\mathbf{r}}_{ji}^t \rangle_j] + \eta \chi_i^t, \tag{2}$$

where $\chi_i^t \in [-\pi/2, \pi/2]$ is an angular white noise drawn from a uniform distribution, η is a parameter setting the strength of the angular noise, $\epsilon_t = \pm 1$ reverses sign with probability rate $k \in [0, 0.5]$, $\hat{\mathbf{r}}_{ji}$ is the unit vector pointing from particle j to i, and the average is taken over the neighbors j within a unit distance of particle i [including i for the alignment, i.e., the first term in (2)]. Pairwise repulsion, modeled here as a torque for convenience, has constant modulus with coupling β. The interaction range is the same for both alignment and repulsion.

Without repulsion ($\beta = 0$), this model, for large reversal rate k, is the minimal model for active nematics introduced in [41] and further studied in [42,43], while without velocity reversals ($k = 0$) it is the Vicsek-style model for "self-propelled rods" of [36]. Figures 1(a) and 1(b) show how the typical (ρ_0, η) phase diagram of these repulsion-free models changes in the presence of repulsion. First, the band-chaos coexistence phase bordering the order-disorder black line is too small to be seen at the system sizes and densities involved. Repulsion induces the emergence of new phases below this black line: For $k = 0.5$ [Fig. 1(b)], arch solutions (described in detail below) *coexist* (in parameter space, not in real space within a solution) with the defect-free nematic liquid at large-enough density (blue region). For rods [$k = 0$, Fig. 1(a)], an *inner* region of

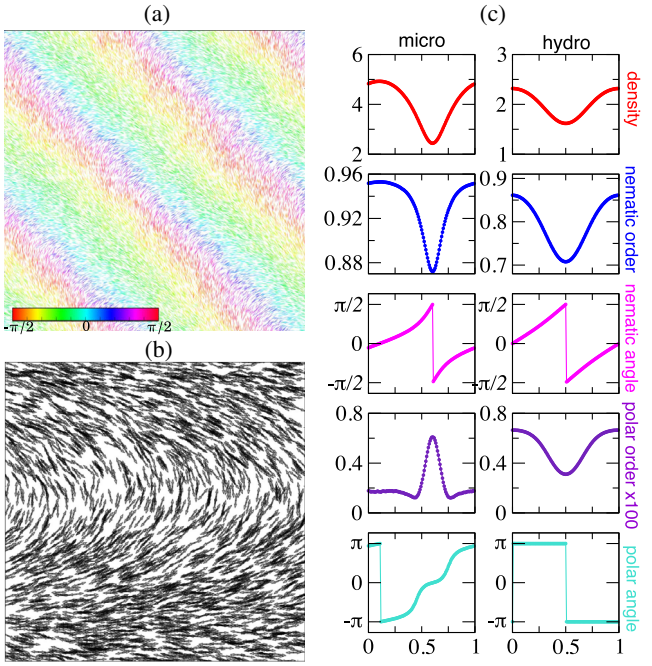

FIG. 2. Arch solutions. (a) snapshot of a steady pattern of arches in the microscopic model ($L = 256$, $\rho_0 = 4$, $v = 0.3$, $\eta = 0.1$, $\beta = 0.5$, $k = 0.5$, particles colored by their orientation). (b) Enlargement of one of the arches seen in (a) (x axis chosen along the arch, particles' orientation marked by double arrows). (c) Profiles of density, nematic, and polar order (modulus and direction) of a single arch [as in (b)] for the microscopic model [left, same parameters as (a)] and the hydrodynamic equations ($\rho_0 = 1$, $a = 10$, $\eta = 0.1$, $b_1 = 0.25$).

nematic chaos (in red) appears deep in the ordered phase [44]. Figures 1(c) and 1(d) show how the two limit cases above ($k = 0$ and $k = 0.5$) are connected when the reversal rate k is varied. In the (ρ_0, k) plane [at $\eta = 0.1$, Fig. 1(c)], the regions of nematic chaos and arch solutions get closer to each other as ρ_0 gets larger. Increasing the system size, the gap in between becomes narrower (not shown). In the (k, η) plane [at $\rho_0 = 4$, Fig. 1(d)], both the nematic chaos region and the arch solutions disappear when approaching the basic isotropic-nematic black transition line.

Nematic chaos is characterized by *local* nematic order but global disorder "mediated" by $\pm\frac{1}{2}$ topological defects (Movie S2 in [45]). It has long but finite correlation lengths and times, and is the result of a longitudinal bending instability of the homogeneous nematic, similar to that observed in the wet case. This instability never saturates into regular undulations, except in small systems. Instead, defects are always nucleated and nematic chaos sets in.

The arch solutions consist of a smectic pattern of rather sharp walls akin to Néel walls or π walls observed in some equilibrium liquid crystals (Fig. 2) [46]. Starting from random initial conditions, local nematic order quickly arises, defects are created, and move across the periodic boundaries. In a large-enough system, this dynamics often

results in some solution comprising several arches, which are found more frequently than the defect-free homogeneous nematic state [Movie S3 in [45], Figs. 2(a) and 2(b)]. Each arch displays local nematic order but is a globally polar object. Particle trajectories show weak but regular drift, with a velocity depending on their position across the arch pattern (Movie S4 in [45]). Characteristic profiles of density, nematic, and drift velocity (polar order) are shown in Fig. 2(c). Arches do *not* have a preferred size: At fixed parameter values, there is a minimal width below which they disappear, but no maximal width. The minimal width varies with parameters (see [45]). They form a regular pattern: A configuration of n arches of various width slowly evolves toward n arches of equal width (Movie S5 in [45]).

To derive hydrodynamic equations for dense active nematics, we start from a Boltzmann equation governing $f(\mathbf{r},\theta,t)$, the probability (density) of finding a particle at position $\mathbf{r}$, with orientation θ, at time t [35,37,47]. This equation extends that used in [47] with a term describing velocity reversals at rate a, as in [43]:

$$\partial_t f + v_0 \mathbf{e}(\theta)\cdot\nabla f = \lambda[\langle f(\theta-\sigma)\rangle_\sigma - f(\theta)] + I_{\mathrm{col}}[f] + a[f(\theta+\pi)-f(\theta)], \tag{3}$$

with λ a tumbling rate, ∇ the gradient operator, and $\langle\cdots\rangle_\sigma$ the average over a noise distribution $P(\sigma)$ (with rms η). The collision integral

$$I_{\mathrm{col}}[f] = \int_{-\pi}^{\pi} d\theta_1 \int_{-\pi}^{\pi} d\theta_2 f(\mathbf{r},\theta_1)\int_0^\infty ds\, s \times \int_{-\pi}^{\pi} d\phi K(s,\phi,\theta_1,\theta_2) f(\mathbf{r}+s\mathbf{e}(\phi),\theta_2) \times [\langle\hat{\delta}(\Psi(\theta_1,\theta_2)+\sigma-\theta)\rangle_\sigma - \hat{\delta}(\theta_1-\theta)], \tag{4}$$

where Ψ is the π-periodic nematic alignment function [$\Psi(\theta_1,\theta_2)=\frac{1}{2}(\theta_2-\theta_1)$ for $-\pi/2<\theta_2-\theta_1<\pi/2$], incorporates the distance-dependent repulsive interaction via the dependence of the collision kernel $K(s,\phi,\theta_1,\theta_2)$ on the relative position $\mathbf{r}'-\mathbf{r}\equiv s\mathbf{e}(\phi)$ of the two colliding particles; $\hat{\delta}$ is a 2π-periodic Dirac distribution. For particles of diameter d_0, the angle ϕ is an impact parameter defined by the position of the contact point at collision. The probability to collide within $[\phi,\phi+d\phi]$ is proportional to $\cos(\phi-\theta_{12})d\phi$, where θ_{12} is the direction of $\mathbf{e}(\theta_1)-\mathbf{e}(\theta_2)$ [collision occurs only if $\cos(\phi-\theta_{12})>0$]. The kernel K reads

$$K = 2g(s)\left|\sin\frac{\theta_1-\theta_2}{2}\right|\cos(\phi-\theta_{12})\Theta[\cos(\phi-\theta_{12})], \tag{5}$$

with $\Theta(x)$ the Heaviside function and $g(s)$ an integrable function over the interval $[0,d_0]$ modeling repulsion between soft spheres [$g(s)=\delta(s-d_0)$ in the hard spheres limit]. The tumbling rate λ and size d_0 can be set to unity. Expanding $f(\mathbf{r}+s\mathbf{e}(\phi),\theta_2)\approx[1+s\mathbf{e}(\phi)\cdot\nabla]f(\mathbf{r},\theta_2)$, the Boltzmann equation is expressed as a hierarchy of equations on complex modes f_k given by $f_k(\mathbf{r})=\int_{-\pi}^{\pi}d\theta e^{\imath k\theta}f(\mathbf{r},\theta)$. Beside the density field $f_0=\rho$, fields of interest are f_1 and f_2 which are related to the polarity vector $\mathbf{P}=(\Re\{f_1\},\Im\{f_1\})$ and nematic tensor $\mathbf{Q}$ [$\mathbf{Q}_{xx}=\Re\{f_2\}$, $\mathbf{Q}_{xy}=\Im\{f_2\}$]. This hierarchy is truncated and closed with the scaling ansatz [47], $\nabla\sim\partial_t\sim\delta\rho\sim\epsilon$, $f_{2k-1}\sim f_{2k}\sim\epsilon^{|k|}$. At order $O(\epsilon^3)$, we obtain the closed equations

$$\partial_t\rho = -\frac{1}{2}v_0(\nabla^* f_1 + \nabla f_1^*), \tag{6}$$

$$\partial_t f_1 = (\alpha[\rho]-\beta|f_2|^2)f_1 + \zeta f_1^* f_2 - \pi_0[\rho]\nabla\rho - \pi_2[\rho]\nabla^* f_2 + \gamma_2 f_2\nabla f_2^* + \gamma_1 f_2^*\nabla f_2 - \lambda_n f_2\nabla*\rho + \lambda_1 f_1\nabla^* f_1 + \lambda_2 f_1\nabla f_1^* + \lambda_3 f_1^*\nabla f_1, \tag{7}$$

$$\partial_t f_2 = (\mu[\rho]+\tau|f_1|^2-\xi|f_2|^2)f_2 + \omega f_1^2 + \nu\triangle f_2 - \pi_1[\rho]\nabla f_1 + \chi_1\nabla^*(f_1 f_2) + \chi_2 f_2\nabla^* f_1 + \chi_3 f_2\nabla f_1^* + \kappa_1 f_1^*\nabla f_2 + \kappa_2 f_1\nabla\rho, \tag{8}$$

where $\nabla=\partial_x+i\partial_y$, $\nabla^*=\partial_x-i\partial_y$, $\triangle=\nabla\nabla^*$. These equations include that for dilute rods [35,47,48]; the last lines in (7) and (8) contain new terms due to repulsion, whose coefficients depend on the first moments of $g(s)$. All coefficients are given in [45]. These equations are formally very close to those obtained when enslaving the fluid in wet active nematics [10,12,13]. A detailed discussion of their structure will be given elsewhere [49]. They possess two uniform solutions: the disordered one ($\rho=\rho_0$, $f_1=f_2=0$), which is stable whenever $\mu[\rho_0]<0$, and the nematically ordered one ($\rho=\rho_0$, $f_1=0$, $|f_2|^2=\mu[\rho_0]/\xi$) for $\mu[\rho_0]>0$, whose full linear stability analysis was performed seminumerically [45]. Without repulsion, and for $a=0$ and $a\to\infty$, we recover the simple phase diagrams found, respectively, in [37,47]. With repulsion (Fig. 3), the transversal "banding" instability region near the $\mu[\rho]=0$ line becomes very thin, and the uniform nematic solution becomes unstable, in the large density, low noise, and low reversal rate region, to a mostly longitudinal bending instability [Fig. 3(a)].

We now study the inhomogeneous solutions of our hydrodynamic equations. As in the microscopic model, the longitudinal bending instability never saturates into stable undulations if the system size is large enough. It always leads to a nematic chaos regime qualitatively similar to that of the particle model (Movie S6 [45]). Where only the homogeneous nematic state is stable, we found no other solution, so that the regions of linear instability described in Fig. 3 are one to one with those of nematic chaos.

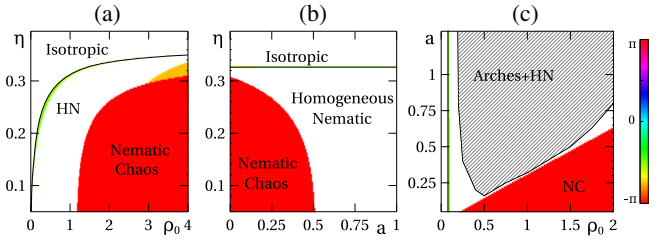

FIG. 3. Phase diagram of hydrodynamic equations. (a) (ρ_0, η) plane for $a = 0.4$. (b) (a, η) plane for $\rho_0 = 1.5$. (c) (ρ_0, a) plane for $\eta = 0.15$. Color map: Angle of most unstable wave vector, if any. The thin green region along the basic order-disorder line is the transverse banding instability. Orange region: Longitudinal bending instability leading to nematic chaos. In the gray region, multiple arch solutions coexist with the homogeneous nematic state [shown only on panel (c)].

Equations (6)–(8) also support stable arch solutions coexisting with the homogeneous nematic state. These solutions are qualitatively similar to those observed in the microscopic model [Fig. 2(c), Movie S7 in [45]]: At given parameter values, arches have a minimal width but no characteristic size. They eventually form a regular smectic pattern. They are globally polar objects with polar drift now encoded explicitly in the f_1 field. Note, however, that the f_1-field profiles are qualitatively different from the polar drift profiles recorded in the microscopic model [Fig. 2(c)], indicating a strong influence on this small field of the approximations made to derive the equations. A careful numerical investigation of the stability domain of arches for a fixed-size system revealed that it is only in rough qualitative agreement with that found in the microscopic model [Fig. 3(c)]. Again, we attribute this difference to the absence of fluctuations: Near the bottom of the gray region in Fig. 3(c), arch solutions are "fragile" and probably do not resist even small amounts of noise. In the particle-based model, all these fragile solutions disappear, leaving the smaller regions of stable arches reported in Figs. 1(c) and 1(d).

We now examine the dynamics of $\pm\frac{1}{2}$ defects in both our microscopic model and hydrodynamic equations. Previous works have investigated defects in the nematic chaos (or nematic turbulence) regime, mostly in wet systems [3–6, 8–10,13,14,17,19–21,30,31]. Here, in an attempt to disentangle the consequences of the linear longitudinal bending instability (leading to chaos) from intrinsic defect properties, we study the dynamics of a $\pm\frac{1}{2}$ defects pair in the uniform nematic state, using parameter values for which this state is the only stable one. In such conditions, the two defects eventually merge and annihilate, since the spontaneous nucleation of a pair is never observed on the scales studied. Increasing system size and the initial distance separating defects they can be observed for very long times. We mostly studied the fate of the configuration shown in Fig. 4(a). For both microscopic model and hydrodynamic equations, the $+\frac{1}{2}$ defect has a well-defined asymptotic velocity v^+ for large separation distance. The $-\frac{1}{2}$ defect has a vanishing velocity in this limit with a diffusive behavior driven by the fluctuations. This is in agreement with previous works. However, the velocity of the $+\frac{1}{2}$ defect depends strikingly on the speed v_0 and the reversal rate: In both microscopic model and hydrodynamic equations, it can even change sign [Fig. 4(b), Movies S8-11 in [45]], whereas $+\frac{1}{2}$ defects were only reported to move with their cap ahead (i.e., upward here) before. (Note though that both signs are considered in [19,21].) We conjecture that in wet active nematics the $+\frac{1}{2}$ defect velocity in the fluid frame might take a different sign depending on swimming speed or reversal rate of the active particles.

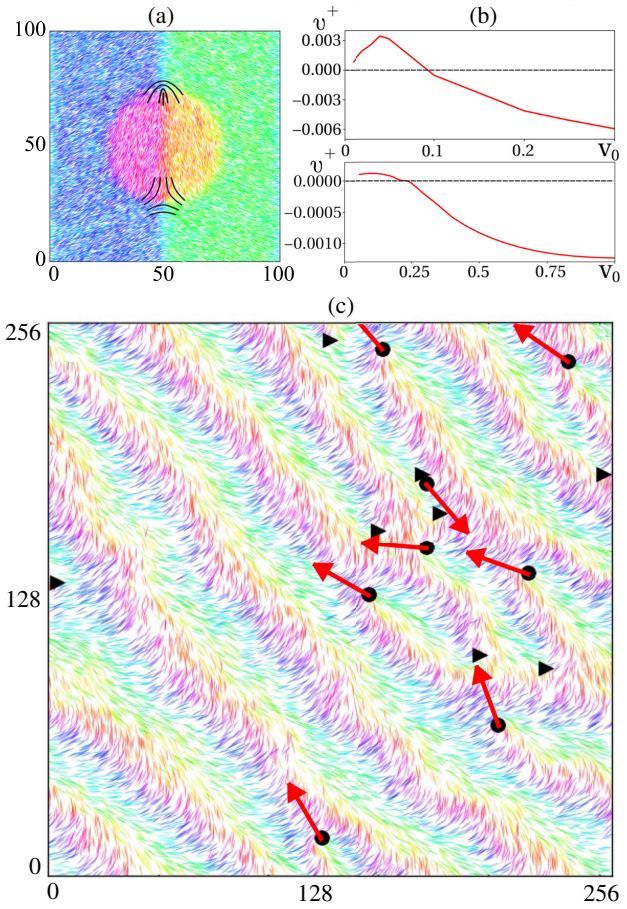

FIG. 4. Defects dynamics and defect ordered states. (a) Typical configuration during initial motion at "asymptotic" velocities (microscopic model). (b) Asymptotic velocity v^+ of the $+\frac{1}{2}$ defect [along the vertical axis in (a)] vs v_0. Top: Microscopic model ($\rho_0 = 4$, $\eta = 0.1$, $\beta = 0.5$, $k = 0.5$). Bottom: Hydrodynamic equations ($\rho_0 = 3$, $\eta = 0.15$, $a = 8.0$, $b_1 = 0.25$). (c) Snapshot of defect ordered state (microscopic model, $\rho_0 = 2$, $v_0 = 0.05$ $\eta = 0.1$, $\beta = 0.5$, $k = 0.5$). Colors as in Fig. 2(a) with superimposed $-\frac{1}{2}$ (triangles) and $+\frac{1}{2}$ defects (circles). The velocities of $+\frac{1}{2}$ defects (red arrows) and their intrinsic orientations (not shown) are globally polarly aligned.

This has direct consequences on the existence of defect ordered states. No such regime was observed at the deterministic hydrodynamic level. This remarkable dynamics arises only for the microscopic model when $v^+ > 0$, for parameter values bordering the domain of observation of arch solutions, where fluctuations are strong enough to nucleate defect pairs. When $v^+ > 0$, freshly created pairs unbind quasideterministically (for $v^+ < 0$, they recombine, but are also perpetually nucleated), and continuously remodel the underlying arch pattern without breaking its global polar order [Fig. 4(c), Movie S12 in [45]]. Thus, the global ordering of $+\frac{1}{2}$ defects—they flock—only reflects that of the nearby arch pattern. This elucidates the origin of the defect ordered state reported for the microscopic model studied in [22] (see also [12,17] for similar, but distinct situations).

To summarize, we have bridged the gap between microscopic and hydrodynamic levels in dense, dry active nematics. The Boltzmann-Ginzburg-Landau approach provides well-behaved hydrodynamic equations whose solutions are in good qualitative agreement with collective states of the original particle model. This comparison was only possible thanks to the expression of hydrodynamic transport coefficients in terms of the microscopic control parameters. With respect to the dilute case, the phase diagram contains two main new features: (i) a large region at low reversal rate where the homogeneous nematic state is unstable at low noise and leaves places to nematic chaos, and (ii) multiple arch solutions that coexist with the nematic state at large reversal rate. These solutions, that are different from structures reported in related context [4,11–13], form globally polar smectic patterns at the origin of the heretofore somewhat mysterious defect ordered states. We also demonstrated that the properties of the ubiquitous $\pm\frac{1}{2}$ topological defects depend strongly on microscopic parameters such as reversal rate and nominal particle speed.

We thank Sandrine Ngo and Esteban Velez for their involvement in the early stages of this work. I. S. A., E. B. and H. C. are grateful to the Max Planck Institute for the Physics of Complex Systems in Dresden (Germany) for hospitality during early developments of the project. Research of I. S. A. was supported by the NSF PHY-1707900.

[1] D. Marenduzzo, E. Orlandini, M. E. Cates, and J. M. Yeomans, Phys. Rev. E **76**, 031921 (2007).
[2] L. Giomi, L. Mahadevan, B. Chakraborty, and M. F. Hagan, Phys. Rev. Lett. **106**, 218101 (2011).
[3] X. Shi and Y. Ma, Nat. Commun. **4**, 3013 (2013).
[4] S. P. Thampi, R. Golestanian, and J. M. Yeomans, Phys. Rev. Lett. **111**, 118101 (2013).
[5] L. Giomi, M. J. Bowick, X. Ma, and M. C. Marchetti, Phys. Rev. Lett. **110**, 228101 (2013).
[6] L. Giomi, M. J. Bowick, P. Mishra, R. Sknepnek, and M. C. Marchetti, Phil. Trans. R. Soc. A **372**, 20130365 (2014).
[7] S. P. Thampi, R. Golestanian, and J. M. Yeomans, Phys. Rev. E **90**, 062307 (2014).
[8] S. P. Thampi, R. Golestanian, and J. M. Yeomans, Phil. Trans. R. Soc. A **372**, 20130366 (2014).
[9] L. Giomi, Phys. Rev. X **5**, 031003 (2015).
[10] A. Doostmohammadi, M. Adamer, S. P. Thampi, and J. M. Yeomans, Nat. Commun. **7**, 10557 (2016).
[11] S. P. Thampi, A. Doostmohammadi, R. Golestanian, and J. M. Yeomans, Europhys. Lett. **112**, 28004 (2015).
[12] P. Srivastava, P. Mishra, and M. C. Marchetti, Soft Matter **12**, 8214 (2016).
[13] E. Putzig, G. S. Redner, A. Baskaran, and A. Baskaran, Soft Matter **12**, 3854 (2016).
[14] A. Doostmohammadi, S. P. Thampi, and J. M. Yeomans, Phys. Rev. Lett. **117**, 048102 (2016).
[15] E. J. Hemingway, P. Mishra, M. C. Marchetti, and S. M. Fielding, Soft Matter **12**, 7943 (2016).
[16] A. J. T. M. Mathijssen, A. Doostmohammadi, J. M. Yeomans, and T. N. Shendruk, J. Fluid Mech. **806**, 35 (2016).
[17] A. U. Oza and J. Dunkel, New J. Phys. **18**, 093006 (2016).
[18] A. Doostmohammadi, J. Ignes-Mullol, J. M. Yeomans, and F. Sagués, Nat. Commun. **9**, 3246 (2018).
[19] S. Shankar, S. Ramaswamy, M. C. Marchetti, and M. J. Bowick, Phys. Rev. Lett. **121**, 108002 (2018).
[20] D. Cortese, J. Eggers, and T. B. Liverpool, Phys. Rev. E **97**, 022704 (2018).
[21] X. Tang and J. V. Selinger, Soft Matter **15**, 587 (2019).
[22] S. J. DeCamp, G. S. Redner, A. Baskaran, M. F. Hagan, and Z. Dogic, Nat. Mater. **14**, 1110 (2015).
[23] S. Zhou, A. Sokolov, O. D. Lavrentovich, and I. S. Aranson, Proc. Natl. Acad. Sci. U.S.A. **111**, 1265 (2014).
[24] A. Creppy, O. Praud, X. Druart, P. L. Kohnke, and F. Plouraboué, Phys. Rev. E **92**, 032722 (2015).
[25] P. Guillamat, J. Ignes-Mullol, and F. Sagues, Proc. Natl. Acad. Sci. U.S.A. **113**, 5498 (2016).
[26] P. Guillamat, J. Ignés-Mullol, S. Shankar, M. C. Marchetti, and F. Sagués, Phys. Rev. E **94**, 060602(R) (2016).
[27] G. Duclos, S. Garcia, H. G. Yevick, and P. Silberzan, Soft Matter **10**, 2346 (2014).
[28] K. Kawaguchi, R. Kageyama, and M. Sano, Nature (London) **545**, 327 (2017).
[29] T. B. Saw, A. Doostmohammadi, V. Nier, L. Kocgozlu, S. Thampi, Y. Toyama, P. Marcq, C. T. Lim, J. M. Yeomans, and B. Ladoux, Nature (London) **544**, 212 (2017).
[30] M. M. Genkin, A. Sokolov, O. D. Lavrentovich, and I. S. Aranson, Phys. Rev. X **7**, 011029 (2017).
[31] M. M. Genkin, A. Sokolov, and I. S. Aranson, New J. Phys. **20**, 043027 (2018).
[32] D. Needleman and Z. Dogic, Nat. Rev. Mater. **2**, 17048 (2017).
[33] I. S. Aranson, Acc. Chem. Res. **51**, 3023 (2018).
[34] H. Li, X.-q. Shi, M. Huang, X. Chen, M. Xiao, C. Liu, H. Chaté, and H. P. Zhang, Proc. Natl. Acad. Sci. U.S.A. **116**, 777 (2019).
[35] A. Peshkov, E. Bertin, F. Ginelli, and H. Chaté, Eur. Phys. J. Spec. Top. **223**, 1315 (2014).
[36] F. Ginelli, F. Peruani, M. Bär, and H. Chaté, Phys. Rev. Lett. **104**, 184502 (2010).

[37] E. Bertin, H. Chaté, F. Ginelli, S. Mishra, A. Peshkov, and S. Ramaswamy, New J. Phys. **15**, 085032 (2013).
[38] T. Vicsek, A. Czirok, E. Ben-Jacob, I. Cohen, and O. Shochet, Phys. Rev. Lett. **75**, 1226 (1995).
[39] H. Chaté, F. Ginelli, G. Grégoire, and F. Raynaud, Phys. Rev. E **77**, 046113 (2008); G. Grégoire and H. Chaté, Phys. Rev. Lett. **92**, 025702 (2004).
[40] P. Romanczuk, H. Chaté, L. Chen, S. Ngo, and J. Toner, New J. Phys. **18**, 063015 (2016).
[41] H. Chaté, F. Ginelli, and R. Montagne, Phys. Rev. Lett. **96**, 180602 (2006).
[42] S. Ngo, A. Peshkov, I. S. Aranson, E. Bertin, F. Ginelli, and H. Chaté, Phys. Rev. Lett. **113**, 038302 (2014).
[43] R. Grossmann, F. Peruani, and M. Bär, Phys. Rev. E **94**, 050602(R) (2016).
[44] At low densities, a small region of *polar* bands with local smectic order is present that quickly disappears for nonzero reversal rates. These bands constitute here a marginal phenomenon.
[45] See Supplemental Material at http://link.aps.org/supplemental/10.1103/PhysRevLett.123.258001 for movies and additional results.
[46] See, e.g., J.-W. Park, J. Cho, and E. L. Thomas, Soft Matter **4**, 739 (2008); A. Sengupta, U. Tkalec, and C. Bahr, Soft Matter **7**, 6542 (2011).
[47] A. Peshkov, I. S. Aranson, E. Bertin, H. Chaté, and F. Ginelli, Phys. Rev. Lett. **109**, 268701 (2012).
[48] E. Bertin, A. Baskaran, H. Chaté, and M. C. Marchetti, Phys. Rev. E **92**, 042141 (2015).
[49] A. Patelli *et al.* (to be published).